PHOTONIC SENSORS / Vol. 7, No. 3, 2017: 234–245

Design and Optimization of Photonic Crystal Fiber Based Sensor for Gas Condensate and Air Pollution Monitoring

Md. Ibadul ISLAM[1], Kawsar AHMED[1,2*], Shuvo SEN[1], Sawrab CHOWDHURY[1], Bikash Kumar PAUL[1,2], Md. Shadidul ISLAM[1], Mohammad Badrul Alam MIAH[1], and Sayed ASADUZZAMAN[1,2,3]

[1]*Department of Information and Communication Technology (ICT), Mawlana Bhashani Science and Technology University, Santosh, Tangail 1902, Bangladesh*

[2]*Group of Bio-photomatiχ, Tangail, 1902, Bangladesh*

[3]*Department of Software Engineering (SWE), Daffodil International University, Sukrabad, Dhaka, 1207, Bangladesh*

[*]Corresponding author: Kawsar AHMED Email: kawsar.ict@mbstu.ac.bd and k.ahmed.bd@ieee.org

Abstract: In this paper, a hexagonal shape photonic crystal fiber (H-PCF) has been proposed as a gas sensor of which both micro-structured core and cladding are organized by circular air cavities. The reported H-PCF has a single layer circular core which is surrounded by a five-layer hexagonal cladding. The overall pretending process of the H-PCF is completed by using a full vectorial finite element method (FEM) with perfectly matched layer (PML) boundary condition. All geometrical parameters like diameters and pitches of both core and cladding regions have fluctuated with an optimized structure. After completing the numerical analysis, it is clearly visualized that the proposed H-PCF exhibits high sensitivity with low confinement loss. The investigated results reveal the relative sensitivity of 56.65% and confinement loss of 2.31×10^{-5} dB/m at the 1.33-μm wavelength. Moreover, effective area, nonlinearity, and *V*-parameter of the suggested PCF are also briefly described**.**

Keywords: Relative sensitivity; confinement loss; gas sensor; effective area; nonlinearity and photonic crystal fiber

Citation: Md. Ibadul ISLAM, Kawsar AHMED, Shuvo SEN, Sawrab CHOWDHURY, Bikash Kumar PAUL, Md. Shadidul ISLAM, *et al*., "Design and Optimization of Photonic Crystal Fiber Based Sensor for Gas Condensate and Air Pollution Monitoring," *Photonic Sensors*, 2017, 7(3): 234–245.

1. Introduction

Photonic crystal fibers (PCFs) have ensured novel modification in the present fiber-optic communication system. It is the perforated fiber that goes through the entire length of fiber. The PCF can be designed for many significant applications in intelligent systems, and it has attracted too much concentration of researchers. The requirement of PCF is exponentially escalated for flexibility and variation of geometrical structures like D-shape [1], pentafgonal [2], tapered [3] panda-shaped [4], colloidal [5], spherical shaped [6], rhombic-shaped core [7], and spiral [8] shaped architecture. High nonlinearity [9], large mode field area [10], highly birefringence [2], and zero-flattened dispersion [11] characteristics have gained by modifying the design of PCF. Distinctive background materials such as Tellurite [12], Topas [13], and Silica [14] are also applied to improve the guiding properties of PCF. As

Received: 13 February 2017/ Revised: 10 March 2017

DOI: 10.1007/s13320-017-0404-6
Article type: Regular

a result, PCF can be utilized in the nanoparticle detection [15], humidity measurement [16], atom-atom interaction [17], micro-organism growth detection [18], bacteria detection [19], air pollution monitoring [14], gas leak detection systems with high accuracy and safety [20], environmental studies [21], sensing [22], and communication systems [23] for its unique optical properties. In recent years, PCFs have established various branches of sensing technology with the promotion of fabrication techniques.

The PCF based sensors are mainly utilized in plasmonic [24], remote irradiation [25], surface, temperature, tension, magnetic field, and gas sensing applications [22]. Nowadays, gas sensing capability of PCF is enhanced rapidly due to its several attractive features like the high relative sensitivity and low confinement loss. The performances of gas sensors are enlarged by changing the size or number of air cavities [26]. The global warming problem is very acute day by day due to various types of toxic gases including C_2H_2, CH_4, NO_2, SO_2, NH_3, H_2S, CO_2, and CO. These combustible and explosive gases are emitted from industries and vehicles. The monitoring and controlling of gas emission are needed to protect our environment from greenhouse effect and global climate change. The PCF-based gas sensors have hastily popular because of low-cost, small footprint, and long interaction length. As a result, it is used in areas such as civil engineering, environment protection, homeland security, and military defense [27].

In previous and current period, the researchers tried their best to upgrade the performance of PCF-based gas sensing technique. Cordeiro *et al.* [28] proposed a microstructure PCF that increased the energy of gas filling air holes. In 2003, Hoo *et al.* [29] reported an all-fiber gas sensor and obtained the relative sensitivity of 10.15% at the 1.4 μm wavelength. The improvement of relative sensitivity of 16.88% and the reduced confinement loss of 1.765×10^{-8} dB/m have been done by Morshed *et al.* [30]. In [31], it suggested an index-guiding PCF and achieved the sensitivity and leakage loss of 29.80% and 4.50×10^{-1} dB/m, respectively. In 2013, Olyaee *et al.* [32] proposed a micro structured PCF and enhanced the sensitivity of 32.99% as well as minimizing the leakage loss of 2.59×10^{-5} dB/m at the 1.33-μm wavelength. Asaduzzaman and Ahmed [14] reported a micro structured elliptical cored photonic crystal fiber (E-PCF) for air pollution monitoring purpose where the core region was constituted with elliptical air holes and exhibited high relative sensitivity, birefringence, and nonlinearity.

In this research paper, we have suggested and successfully scrutinized a hexagonal photonic crystal fiber (H-PCF) where five-layer hexagonal cladding and single layer circular core territories are formed by circular air holes. The proposed H-PCF is mentioned as a gas sensor that improves the relative sensitivity of 56.65% and reduces the confinement loss of 2.31×10^{-5} dB/m at $\lambda=1.33$ μm. In addition, the effective area and nonlinearity of 6.44 μm^2 and 22.73 $W^{-1}\cdot km^{-1}$ respectively are gained at the same wavelength. So, the reported PCF is massively efficient for pollution monitoring applications and it ensures the industrial safety.

2. Geometries of the proposed H-PCF

Figure 1 depicts the transverse cross-sectional view of the proposed H-PCF based on micro-structured core and cladding in circular and hexagonal manner, respectively. This technique was applied in [33] where the cladding region was hexagonal with six type's holes in the edges of the outermost cladding. In the work, the diameters of two outermost rings as well as three innermost rings were different. In our proposed H-PCF, the diameters of all five rings of cladding have been kept the same to interact the proper fabrication tolerance, which were defined as d [14]. The idea of the micro-structured core was introduced in [34]. In the proposed design, the angular displacement of two adjacent air holes in the cladding region is kept

60° to form a hexagonal structure. The dimensions of air holes in the core are smaller than that of cladding holes to satisfy the effective index guiding criterion. In our H-PCF, the micro-structured core is formed with an array of eight tiny air holes in circular manner, the diameter is defined as d_c, and the diameter of supplementary center air hole in the core region is d_{c0}. The distance between center to center of holes is called pitch of cladding denoted as Λ. The distance from center to the first air hole ring in the core region is defined as Λ_c. Due to the central hole, the refractive indices between core and cladding dropped and more light would confine into the core, thereby the sensitivity increases. To gain more relative sensitivity, the innermost ring is formed with six air holes in hexagonal manner closer to the core region [35]. The effect of the size, position, and shape of those holes on the sensitivity and confinement loss are numerically investigated by applying different numerical methods.

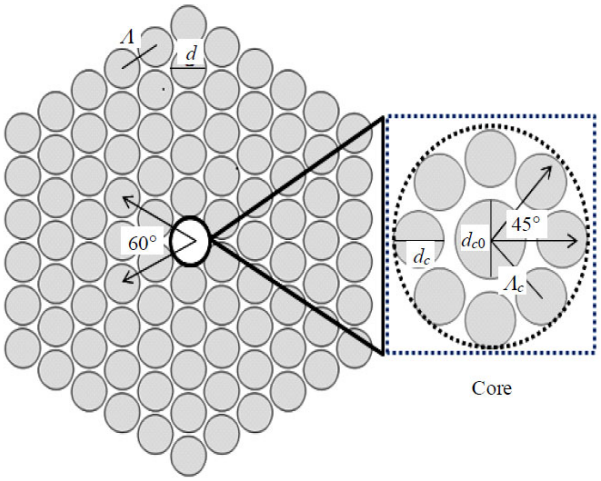

Fig. 1 Transverse cross-sectional view of the proposed H-PCF.

3. Synopsis of numerical method

The finite element method (FEM) is applied for solving Maxwell's equations due to correctly pretending the optical properties of the suggested H-PCF. Moreover, it has capacity to solve the complex architectural design of PCF and also contributes full vector analysis of distinctive PCF structures [36]. As a result, it provides a good approximation to prove the reliability of PCF structures. It is known that due to the finite number of air holes in the cladding, light can leak among the air holes called the leakage loss or confinement loss. So, to compute the leakage loss, an effective boundary condition which produces no reflection at the boundary is needed. In this case, perfectly matched layers (PMLs) are the most efficient absorption boundary condition for this purpose [37–38]. The confinement loss or leakage loss can be calculated as [14]

$$L_C = 8.868 \times K_0 \,\mathrm{Im}[n_{\mathrm{eff}}](\mathrm{dB/m}) \tag{1}$$

where $k_0 = 2\pi/\lambda$; λ is the wavelength of light, and Im[n_{eff}] is the imaginary part of the refractive index.

Beer-Lambert law is used to evaluate the absorbance of evanescent field by the gas samples. The relationship between gas concentration and optical intensity is evaluated as [14]

$$I(\lambda) = I_0(\lambda)\exp[-r\alpha_m l_c] \tag{2}$$

where I and I_0 are the output and input light intensities, respectively, α_m is the absorption coefficient, l is the length of the H-PCF used for chemical detection, c is the concentration of the target samples, and r is a relative sensitivity coefficient defined as [34]

$$r = \frac{n_r}{n_{\mathrm{eff}}} \times f \tag{3}$$

where n_r are the refractive index of gas, n_{eff} is the real part of the effective mode index, and f is the fraction of the total power located in the holes that can be expressed as [34]

$$f = \frac{\int_{\mathrm{sample}} \mathrm{Re}(E_x H_y - E_y H_x)dxdy}{\int_{\mathrm{total}} \mathrm{Re}(E_x H_y - E_y H_x)dxdy} \times 100 \tag{4}$$

where E_x, E_y, H_x, and H_y are the transverse electric and magnetic fields of the guided mode, respectively.

Utilizing the Sellmeier's equation [14], pure silica is set as the background material of the fiber of which the refractive index changes with the modification of the wavelength.

$$n(\lambda)=\sqrt{\left(1+\frac{B_1\lambda^2}{\lambda^2-c_1}+\frac{B_2\lambda^2}{\lambda^2-c_2}+\frac{B_3\lambda^2}{\lambda^2-c_3}\right)} \quad (5)$$

where B_1, B_2, B_3, C_1, C_2, and C_3 are the Sellmeier's coefficients. The refractive index of silica is $n(\lambda)$ which alters with the operating wavelength.

The V-parameter [39] is used to compute the single mode response of a fiber which can be defined as

$$V_{\text{eff}}=\frac{2\pi\Lambda}{\lambda}\sqrt{n_{c0}^2-n_{cl}^2} \quad (6)$$

where the refractive indices of core and cladding regions are denoted by n_{c0} and n_{cl}, respectively. To fulfill the single mode condition, the value of V_{eff} must be not greater than 2.405. Another important parameter is effective area (A_{eff}) which can be determined by the following equation [14]:

$$A_{\text{eff}}=\frac{\left(\iint|E|^2\,dxdy^2\right)}{\iint|E|^4\,dxdy} \quad (7)$$

where optical power is denoted by E. Equation (8) is applied to determine the nonlinear coefficient (γ) [14]

$$\gamma=\left(\frac{2\pi}{\lambda}\right)\left(\frac{n_2}{A_{\text{eff}}}\right) \quad (8)$$

where n_2 is called the nonlinear refractive index.

In this research, the main focus is on the methane (CH_4) and hydrogen fluoride (HF) gasses to have the absorption line at the wavelength of 1.33 μm. We have tried to improve the relative sensitivity and confinement loss at this wavelength. Furthermore, for the other wavelength, our proposed H-PCF has shown the better results.

4. Numerical results and discussion

FEM for disposing Maxwell's equations has been used for its reliability as well as high accuracy to investigate the optical properties of the proposed H-PCF [40–41]. Full vectorial FEM with the perfectly match layer (PML) boundary condition is one of the most potential numerical approaches. It is the most obtainable approach to engineer for structuring and developing photonic elements and devices [42]. To investigate propagation properties of leaky modes, the PML as boundary conditions is an essential approach in PCFs and by employing these layers, all optical propagation characteristics can be appraised in a single run [41, 43, 44]. Figure 2 exhibits the fundamental mode field distributions along x-polarization [Fig. 2(a)] and y-polarization [Fig. 2(b)] for the proposed H-PCF at the operating wavelength of 1.33 μm. From this figure, it is evaluated that the Gaussian distribution of the fields is uniform as well as the fundamental modes which are strongly bounded by the core region of circular air holes. It also illustrates that the sample air holes close to the core region strongly interacts with the evanescent field that causes the high sensitivity as well as low confinement loss.

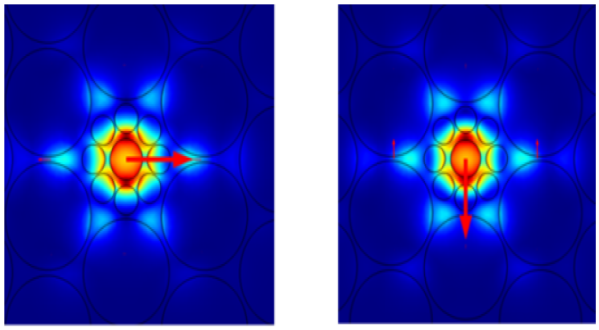

(a) (b)

Fig. 2 Modal intensity distribution of the proposed H-PCF at the wavelength of 1.33 μm: (a) x-polarization and (b) y-polarization.

Due to the increment of air hole diameter of innermost ring of cladding, the fraction of evanescent field penetrates into core that improves relative sensitivity [33]. Figure 3 represents the relative sensitivity versus wavelength curve [Fig. 3(a)] and confinement loss versus wavelength curve [Fig. 3(b)] for the optimized parameters of the proposed structure and investigates the behavior of guiding properties. A simple technique is used to optimize the parameters and figure out x-polarized mode to acquire optimum results. By selecting a proper mode of mesh size, the simulation task has been completed by applying 4.2 version COMSOL Multiphysics [14].

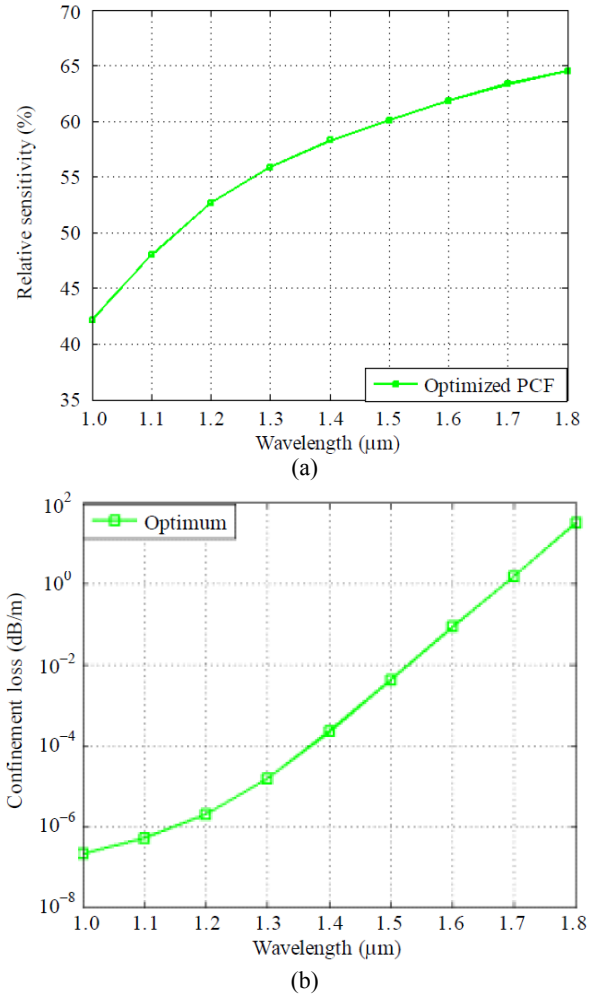

Fig. 3 Relationship between: (a) relative sensitivity versus wavelength and (b) confinement loss versus wavelength curve for the proposed H-PCF for optimized parameters: $\Lambda=3.00$ μm, $\Lambda_c=1.08$ μm, $d=2.85$ μm, $d_c=0.774$ μm, and $d_{c0}=1.08$ μm.

As the penetrating field in the cladding is unloading, inner rings have higher impact on sensitivity; so it is enhanced for the diameter of air holes in the innermost ring as much as possible. It can be seen that 56.65% relative sensitivity as well as 2.31×10^{-5} dB/m confinement loss can be obtained at the operating wavelength of 1.33 μm. From the observation, it can be seen that the proposed H-PCF has a higher relative sensitivity compared with prior PCFs [14, 30–32, 34].

For the central air holes, when enough light would be confined into the cladding region and interaction happens between light and gases, then sensitivity will be increased [31]. The air filling ratio (d/Λ) of 0.95 is acceptable for fabrication [45], and we have carefully optimized all these parameters. Figure 4 describes the variations of air filling ration (d/Λ) in cladding by keeping other parameters fixed to $\Lambda=3.00$ μm, $\Lambda_c=1.08$ μm, $d_c=0.774$ μm, and $d_{c0}=1.08$ μm. At the operating wavelength 1.33 μm, the air filling ratio d/Λ is defined as 0.94, 0.95, and 0.96, the considered relative sensitivities are 55.21%, 56.65%, and 57.86%, and confinement losses are 5.08×10^{-4} dB/m, 2.31×10^{-5} dB/m, and 3.41×10^{-6} dB/m, respectively.

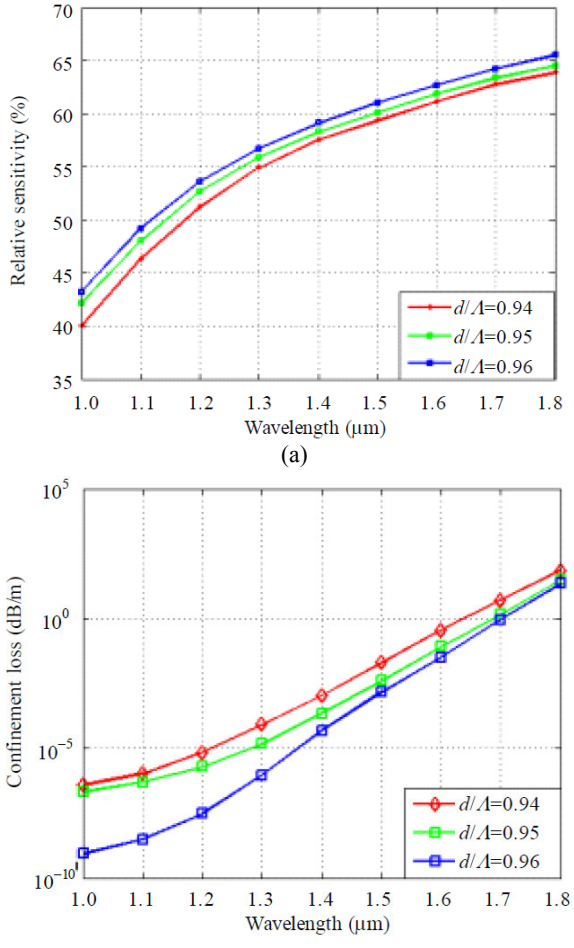

Fig. 4 Comparison between: (a) relative sensitivity versus wavelength and (b) confinement loss versus wavelength curve of the proposed H-PCF for optimized parameters: $\Lambda=3.00$ μm; $\Lambda_c=1.08$ μm; $d_c=0.774$ μm and $d_{c0}=1.08$ μm; $d/\Lambda=0.94$, 0.95, and 0.96.

By the reduction of air filling ratio d/Λ, the evanescent field penetrated into cladding causes the fraction power of holes alleviates and leads to a decrease in the absorption power by core region which causes the relative sensitivity to decrease. On

the other hand, if the air filling ratio (d/Λ) is promoted, the evanescent field penetrating into core region causes an increase in the fraction power of holes which leads to an increase in the absorption power by core region so as to enhance the relative sensitivity. The higher sensitivity makes a fiber as an active candidate to detect noxious gas, colorless gas, and monitor environment pollution [14]. Now d/Λ= 0.95 is selected as an optimized value for the further investigation process.

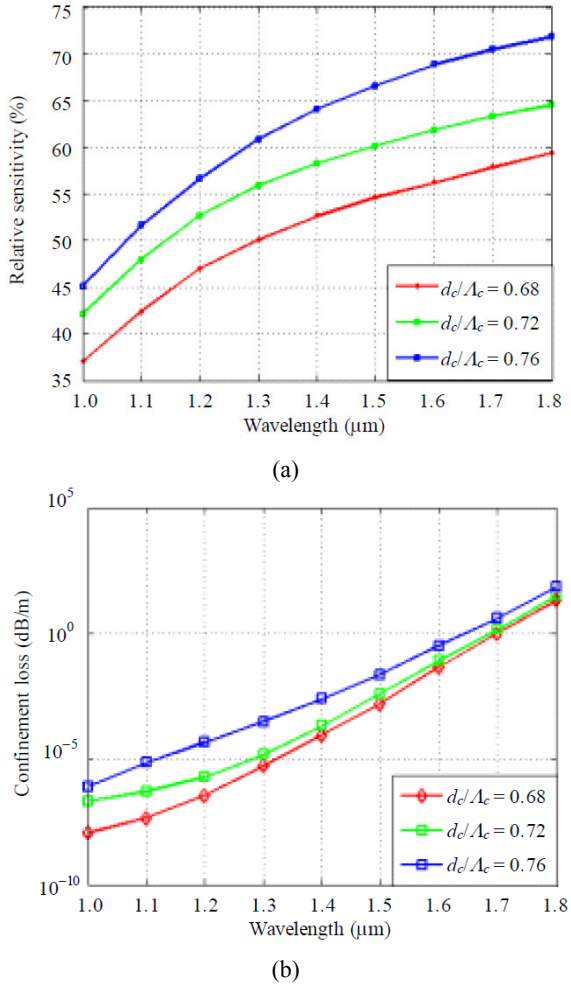

Fig. 5 Comparison between: (a) relative sensitivity versus wavelength and (b) confinement loss versus wavelength curve for the proposed H-PCF for optimized parameters: Λ=3.00 μm; Λ_c=1.08 μm; d=2.85 μm and d_{c0}=1.08 μm; d_c/Λ_c=0.68, 0.72, and 0.76.

The micro-structured core PCFs help gain higher relative sensitivity and alleviate confinement loss [36]. Besides, it can be analyzed that the relative sensitivity is promoted with the enhancement of air holes diameter in the core region and decrement of pitch Λ_c [30]. Figure 5 shows the effect of air filling ratio d_c/Λ_c of core region when other parameters are kept fixed. At the wavelength 1.33 μm, the variations of d_c/Λ_c are defined as 0.68, 0.72, and 0.76, and the calculated relative sensitivities are 51.28%, 56.65%, and 62.47%, respectively. At the same wavelength, the considered confinement losses are 8.53×10^{-6} dB/m, 2.31×10^{-5} dB/m, and 7.56×10^{-4} dB/m, respectively. It can be also mentioned that the evanescent field can be absorbed into the core region by promoting air filling ratio (d_c/Λ_c) which leads to enhancing the absorption power and causes high sensitivity as well as low confinement loss. Besides, the capability of core to confine the power fraction is low when the air filling ration d_c/Λ_c decreases.

Now to obtain the expected result, the pitch is chosen as Λ=2.18 μm for optimizing the investigation process. The variation of pitch (Λ) has great effect on relative sensitivity. High sensitivity makes the fiber more practical in the sensing applications like toxic and colorless gas detection [30]. The relative sensitivity versus wavelength curve for variations of pitch (Λ) of cladding is depicted in Fig. 6(a) when other parameters (Λ_c = 1.08 μm; d=2.85 μm, and d_c=0.774 μm, and d_{c0}= 1.08 μm) are kept constant. According to the variation of Λ as 2.96 μm, 3.00 μm, and 3.04 μm, the calculated relative sensitivities are 57.11%, 56.65%, and 54.32% and confinement losses [Fig. 6(b)] are 3.23×10^{-6} dB/m, 2.31×10^{-5} dB/m, and 9.18×10^{-4} dB/m, respectively. From the above observation, it can be mentioned that the higher relative sensitivity can be gained by reducing pitch of cladding Λ as much as possible [33]. In another sense, it can be mentioned that if Λ is enhanced, the evanescent field would not be confined properly into core. So the power fraction of holes alleviates which governs to decrease the absorption power by core region and the relative sensitivity decays. From Fig. 6(b), it is visualized that the confinement loss is decreases by enhancing pitch [34].

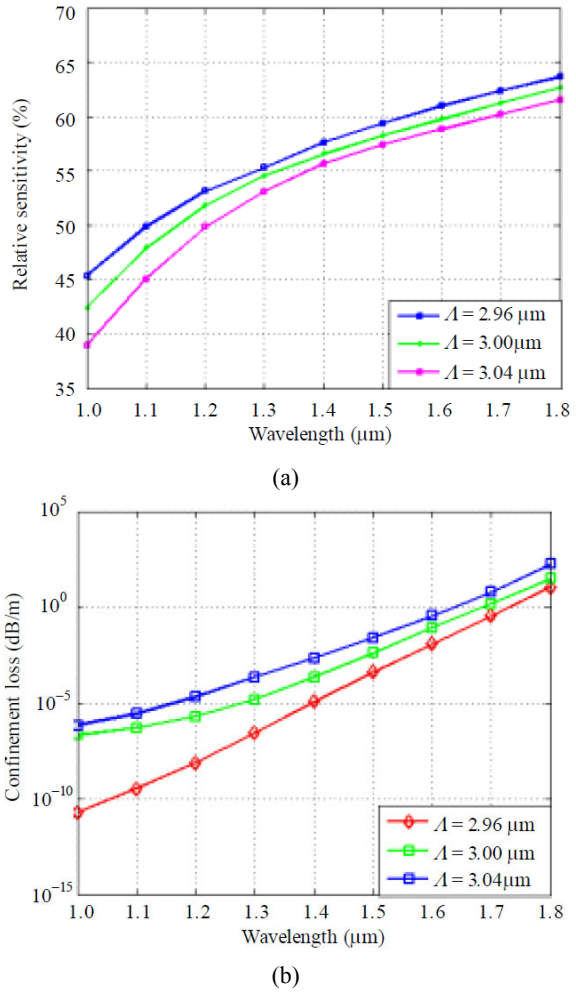

Fig. 6 Comparison between: (a) relative sensitivity versus wavelength and (b) confinement loss versus wavelength curve for the proposed H-PCF for optimized parameters: Λ=2.96 μm, 3.00 μm and 3.04 μm; Λ_c=1.08 μm; d=2.85 μm, d_c=0.774 μm, and d_{c0}=1.08 μm.

Figure 7 exhibits the effect of pitch variations of core on relative sensitivity and confinement loss by keeping other parameters fixed. From this figure, it is observed that the relative sensitivity enhances and the confinement loss alleviates when the pitch of core decreases and vice versa. From observations (Fig. 7), Λ_c = 1.08 μm is selected for further processing. To improve the relative sensitivity and confinement loss simultaneously, the diameter of central air hole should be increased as much as possible [45]. Figure 8 describes the effect of diameter of central air hole on relative sensitivity and the confinement loss. At the operating wavelength 1.33 μm, the considered relative sensitivities are 53.35%, 56.65%, and 59.68%, and confinement losses are 8.73×10^{-6} dB/m, 2.31×10^{-5} dB/m, and 6.75×10^{-4} dB/m, respectively.

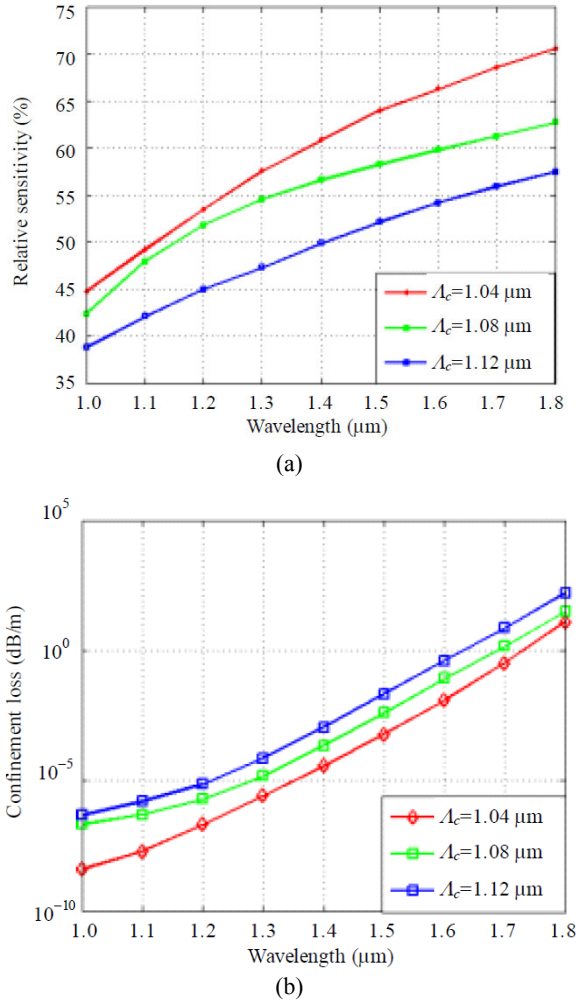

Fig. 7 Comparison between: (a) relative sensitivity versus wavelength and (b) confinement loss versus wavelength curve for the proposed H-PCF for optimized parameters: Λ=3.00 μm; Λ_c=1.04 μm, 1.08 μm, and 1.12 μm; d=2.85 μm, d_c=0.774 μm, and d_{c0}=1.08 μm.

Figure 9 illustrates the effective area and nonlinear coefficient of the proposed H-PCF as a function of wavelength for the optimized parameters as Λ = 3.00 μm, Λ_c = 1.08 μm, d = 2.85 μm, d_c = 0.774 μm, and d_{c0} = 1.08 μm. It is noticed that effective area enhances according to the increment of wavelength. The mode power is narrowly demarked in the core region at longer wavelength, so the guiding waves diverse largely. As a result, the propagating modes hold a larger effective area [46]. A reverse relationship can be seen for the nonlinear

coefficient, which is also depicted in Fig. 9. The effective area and nonlinear coefficient of 6.44 μm^2 and 22.73 W^{-1}·km^{-1} have been achieved respectively at λ=1.33 μm.

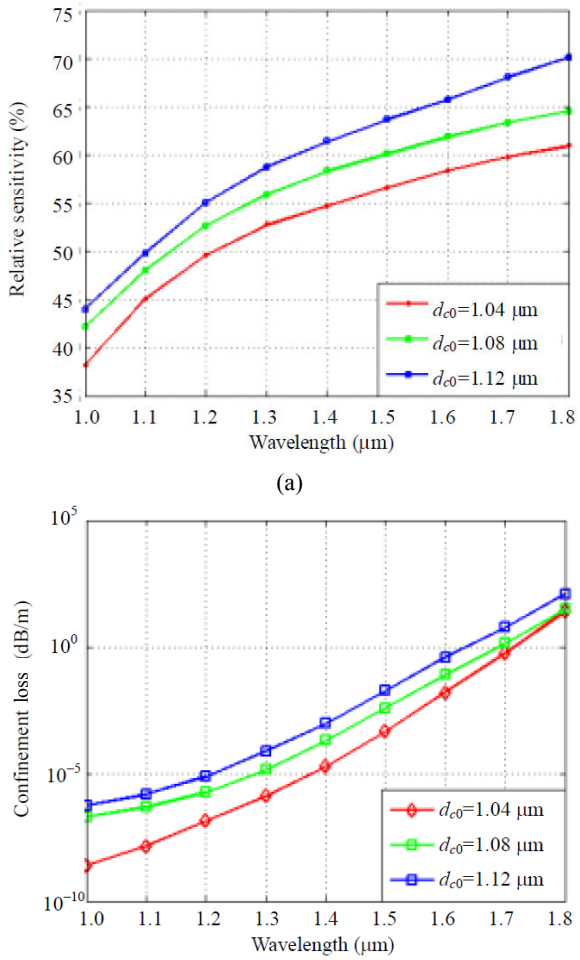

Fig. 8 Comparison between: (a) relative sensitivity versus wavelength and (b) confinement loss versus wavelength curve for the proposed H-PCF for optimized parameters: Λ=3.00 μm; Λ_c = 1.08 μm; d = 2.85 μm, d_c = 0.774 μm, and d_{c0} = 1.04 μm, 1.08 μm, and 1.12 μm.

The single-mode operation of the proposed H-PCF using V effective (V_{eff}) parameter can be investigated. Figure 10 shows the V_{eff} parameter as a function of operating wavelength with optimized design parameters for Λ=3.00 μm; Λ_c=1.08 μm; d= 2.85 μm, d_c = 0.774 μm, and d_{c0} = 1.08 μm. The V_{eff} parameter can be expressed by (6). With approximate perfect electric and perfect magnetic conductor boundary condition, FEM is used at the outer enclosure to achieve the index of space-filling mode [39]. At operating wavelength 1.33 μm, the desired agreement for operating as an SMF is $V_{\text{eff}} \leq$ 2.405 [14]. From Fig. 10, it is visualized that the gained V_{eff} value is 0.95 at wavelength 1.33 μm which is less than 2.405. From above observations, it can clearly be mentioned that the fiber remains constant to single mode over the entire bands.

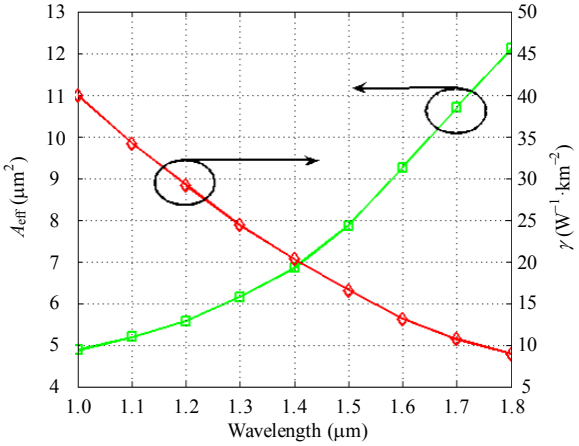

Fig. 9 Effective area and nonlinear coefficient of the x-polarization mode of the proposed H-PCF as a function of wavelength for Λ= 3.00 μm; Λ_c = 1.08 μm; d = 2.85 μm, d_c = 0.774 μm, and d_{c0} = 1.08 μm.

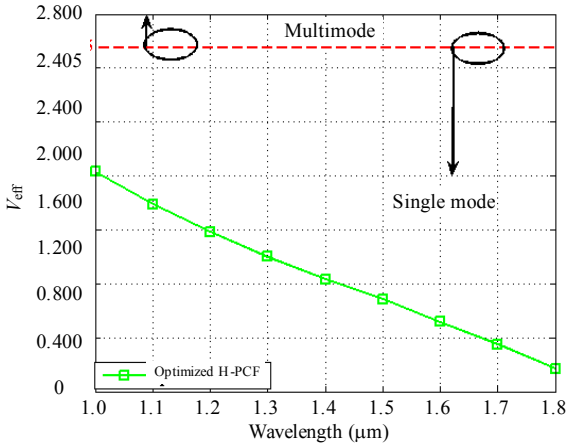

Fig. 10 V parameter of the proposed H-PCF as a function of wavelength for Λ = 3.00 μm, Λ_c = 1.08 μm, d= 2.85 μm, d_c = 0.774 μm, and d_{c0} = 1.08 μm.

After completing numerical investigation, the effects of distinguished parameters on the proposed hexagonal photonic H-PCF are observed. It is evidently reported that the relative sensitivity can be promoted due to the decrement of global diameter shown in Table 1. High sensitivity leads to confine more light into core region as well as better electromagnetic power interaction with gasses.

Table 1 also exhibits the effect of changing global parameters of ±1% and ±2%, on confinement loss, effective area, and nonlinearity. It is noticed that the effective area promotes with an increase in air holes diameter as well as a decrease in the non-linear coefficient.

Table 1 Comparison of different index-guiding properties for optimum design parameters and also for fiber's global diameter variations of order ± 1 % – ± 2 % around the optimum value.

Change in diameters (%)	Relative sensitivity (%)	Confinement loss (dB/m)	A_{eff} (μm^2)	γ ($W^{-1}\cdot km^{-1}$)
+2	55.44	1.71×10^{-5}	7.46	19.63
+1	56.37	2.10×10^{-5}	6.47	22.63
Optimum	56.65	2.31×10^{-5}	6.44	22.73
–1	56.93	6.43×10^{-5}	6.29	23.28
–2	57.21	6.83×10^{-5}	6.25	23.43

Table 2 demonstrates the comparison among relative sensitivity, confinement loss, effective area, and nonlinearity of the proposed H-PCF with other prior designs in [14, 30, 34, 40, 45]. The proposed H-PCF provides about 56.65% sensitivity as well as low confinement loss at the 1.33 μm wavelength. Besides, the reported H-PCF shows higher effective area and nonlinear coefficient at the same wavelength compare to prior PCFs.

Table 2 Comparison of simulated results among proposed PCF and prior PCFs at 1.33 μm wavelength.

PCFs	Relative sensitivity (%)	Confinement loss (dB/m)	A_{eff} (μm^2)	γ ($W^{-1}\cdot km^{-1}$)
Ref. [34]	15.67	1.12×10^{-7}		
Ref. [30]	16.88	1.765×10^{-8}		
Ref. [40]	20.10	1.09×10^{-3}	-	-
Ref. [45]	48.26	1.26×10^{-5}	4.02	
Ref. [14]	53.07	3.21×10^{-6}	3.88	15.67
Proposed PCF	56.65	2.31×10^{-5}	6.44	22.73

Finally, the fabrication process is one of the fundamental issues in PCFs. In the proposed H-PCF three mixing air-holes are considered and shown in Fig. 1. Different methods have been offered for the fabrication of micro-structured fibers such as stack and draw [47], drilling [48], sol-gel casting [49], and extrusion [50] methods. Triangular or honeycomb lattices can be fabricated by stack and draw methods but cannot easily generate circular patterns. The drilling methods offer adjustment of both holes size and spacing but are usually limited to a few number of holes and bounded to circular shapes. Extrusion techniques permit design freedom, but are typically restricted for soft glasses because those cause the material loss with severely high values. However, the proposed structure can be fabricated by currently developed technology for technological advancement in the fabrication of PCFs [51]. El *et al*. [49] provided a sol-gel technique to fabricate the PCFs with all structures, and they provide the freedom to adjust air-hole size, shape, and spacing. In such situation, our proposed H-PCF can be fabricated by the sol-gel casting method. After drawing the relative sensitivity curve to the expected level in the way just illustrated, we then verify the accuracy of the property of the proposed design. A standard fiber draw, ±1% variations in fiber global diameter may occur during the fabrication process.

5. Conclusions

Two major propagation characteristics like the relative sensitivity and confinement loss of an optical sensor have been numerically examined in this paper. The reported optical sensor acts as a gas sensor which has five layers hexagonal cladding with circular shape core. Compared with the prior reported PCFs, our proposed H-PCF exposes high relative sensitivity with low confinement loss. After finishing all investigations, the relative sensitivity and confinement loss of 56.65% and 2.31×10^{-5} dB/m correspondingly are gained at the 1.33 μm wavelength. Moreover, the effective area of 6.44 μm^2 and nonlinearity of 22.73 $W^{-1}\cdot km^{-1}$ are achieved at the same wavelength. So, it is expected that the reported H-PCF will be efficient in gas sensing applications as well as greatly beneficial for the gas detection in industrial sectors and safety purpose with high accuracy.

References

[1] H. J. Kim, O. Kown, S. B. Lee, and Y. Han, "Measurement of temperature and refractive index based on surface long-period gratings deposited onto a d-shaped photonic crystal fiber," *Applied Physics B*: *Chemical,* 2010, 102(1): 81–85.

[2] F. Yu, Z. P. Wang, W. H. Yang, and C. Y. Lv, "Characteristics of highly birefringent photonic crystal fiber with defected core and equilateral pentagon architecture," *Advances in OptoElectronics*, 2016, 2016(6): 1–8.

[3] E. C. Mägi, P. Steinvurzel, and B. J. Eggleton, "Tapered photonic crystal fibers," *Optics Express*, 2004, 12(5): 776.

[4] S. L. Mousavi and M. Sabaeian, "Thermal stress-induced depolarization loss in conventional and panda-shaped photonic crystal fiber lasers," *Brazilian Journal of Physics*, 2016, 46(5): 481–488.

[5] S. H. Kim and G. R. Yi, "Colloidal photonic crystals for sensor applications," *Photonic Materials for Sensing, Biosensing and Display Devices*, 2016, 229: 51–78.

[6] H. P. Gong, M. L. Xiong, Z. H. Qian, C. L. Zhao, and X. Y. Dong, "Simultaneous measurement of curvature and temperature based on Mach-Zehnder interferometer comprising core-offset and spherical-shape structures," *IEEE Photonics Journal*, 2016, 8(1): 1–9.

[7] H. L. Bao, K. Nielsen, H. K. Rasmussen, P. U. Jepsen, and O. Bang, "Fabrication and characterization of porous-core honeycomb bandgap THz fibers," *Optics Express*, 2012, 20(28): 29507–29517.

[8] M. I. Islam, M. Khatun, S. Sen, K. Ahmed, and S. Asaduzzaman, "Spiral photonic crystal fiber for gas sensing application," in *Proceeding of IEEE 9th International Conference on Electrical and Computer Engineering*, Dhaka, Bangladesh, 2016, pp. 20–22.

[9] J. Han, S. Y. Li, and T. Zhang, "Design on a novel hybrid-core photonic crystal fiber with large birefringence and high nonlinearity," *Optical and Quantum Electronics*, 2016, 48(371): 1–11.

[10] B. K. Paul, K. Ahmed, S. Asaduzzaman, and M. S. Islam, "Folded cladding porous shaped photonic crystal fiber with high sensitivity in optical sensing applications: design and analysis," *Sensing and Bio-Sensing Research*, 2017, 12(1): 36–42.

[11] W. C. Cai, E. Liu, B. Feng, H. F. Liu, Z. M. Wang, W. Xiao, *et al.*, "Dispersion properties of a photonic quasi-crystal fiber with double cladding air holes," *Optik – International Journal for Light and Electron Optics*, 2016, 127(10): 4438–4442.

[12] Z. L. Liu, J. An, J. W. Xing, and H. L. Du, "Polarization rotator based on liquid crystal infiltrated tellurite photonic crystal fiber," *Optik – International Journal for Light and Electron Optics*, 2016, 127(10): 4391–4395.

[13] A. Argyros, "Microstructures in polymer fibers for optical fibers, THz waveguides, and fiber-based metamaterials," *ISRN Optics*, 2013, 2013(7): 1–22.

[14] S. Asaduzzaman and K. Ahmed, "Proposal of a gas sensor with high sensitivity, birefringence and nonlinearity for air pollution monitoring," *Sensing and Bio-Sensing Research*, 2016, 10: 20–26.

[15] D. Q. Yang, W. Yuan, and Y. F. Ji, "Nanoparticle detection using fano-resonance photonic crystal on optical fiber-tip," *SPIE*, 2016, 10158: 10158l1–10158l8.

[16] S. Rota-Rodrigo, A. Lopez-Aldaba, R. A. Perez-Herrera, M. D. L. Bautista, O. Esteban, and M. Lopez-Amo, "Simultaneous measurement of humidity and vibration based on a microwire sensor system using fast Fourier transform technique," *Journal of Lightwave Technology*, 2016, 34(19): 4525–4530.

[17] J. D. Hood, A. Goban, A. Asenjo-Garcia, M. Lu, S. P. Yu, D. E. Chang, *et al*., "Atom-atom interactions around the band edge of a photonic crystal waveguide," *Proceedings of the National Academy of Sciences*, 2016, 113(38): 10507–10512.

[18] X. H. Liu, M. S. Jiang, Q. M. Sui, S. Y. Luo, and X. Y. Geng, "Optical fiber Fabry-Perot interferometer for microorganism growth detection," *Optical Fiber Technology*, 2016, 30: 32–37.

[19] E. Brzozowska, M. Koba, M. Smietana, S. Gorska, M. Janik, A. Gamian, *et al.*, "Label-free gram-negative bacteria detection using bacteriophage-adhesin-coated long-period gratings," *Biomedical Optics Express*, 2016, 7(3): 829.

[20] Z. Yang, M. L. Liu, M. Shao, and Y. J. Ji, "Research on leakage detection and analysis of leakage point in the gas pipeline system," *Open Journal of Safety Science and Technology*, 2011, 01(03): 94–100.

[21] M. F. H. Arif, S. Asaduzzaman, M. J. H. Biddut, and K. Ahmed, "Design and optimization of highly sensitive photonic crystal fiber with low confinement loss for ethanol detection," *International Journal of Technology*, 2016, 6: 1068–1076.

[22] K. Ahmed and M. Morshed, "Design and numerical analysis of microstructured-core octagonal photonic crystal fiber for sensing applications," *Sensing and Bio-Sensing Research*, 2016, 7(1): 1–6.

[23] F. Du, Y. Q. Lu, and S. T. Wu, "Electrically tunable liquid-crystal photonic crystal fiber," *Applied Physics Letters*, 2004, 85(12): 2181.

[24] A. A. Rifat, R. Ahmed, A. K. Yetisen, H. Butt, A. Sabouri, G. A. Mahdiraji, *et al.*, "Photonic crystal fiber based plasmonic sensors," *Sensors and*

Actuators B: Chemical, 2017, 243: 311–325.
[25] R. Zeltner, D. S. Bykov, S. Xie, T. G. Euser, and P. S. J. Russell, "Fluorescence-based remote irradiation sensor in liquid-filled hollow-core photonic crystal fiber," *Applied Physics Letters*, 2016, 108(23): 231107.
[26] S. H. Kassani, R. Khazaeinezhad, Y. Jung, J. Kobelke, and K. Oh, "Suspended ring-core photonic crystal fiber gas sensor with high sensitivity and fast response," *IEEE Photonics Journal*, 2015, 7(1): 1–9.
[27] S. J. Zheng, M. Ghandehari, and J. P. Ou, "Photonic crystal fiber long-period grating absorption gas sensor based on a tunable erbium-doped fiber ring laser," *Sensors and Actuators B: Chemical*, 2016, 223: 324–332.
[28] C. M. B. Cordeiro, M. A. Franco, G. Chesini, E. C. Barretto, R. Lwin, C. B. Cruz, *et al.*, "Microstructured-core optical fibre for evanescent sensing applications," *Optics Express*, 2006, 14(26): 13056.
[29] Y. L. Hoo, W. Jin, C. Shi, H. L. Ho, D. N. Wang, and S. C. Ruan, "Design and modeling of a photonic crystal fiber gas sensor," *Applied Optics*, 2003, 42(18): 3509.
[30] M. Morshed, M. I. Hasan, and S. M. A. Razzak, "Enhancement of the sensitivity of gas sensor based on microstructure optical fiber," *Photonic Sensors*, 2015, 5(4): 312–320.
[31] Z. G. Zhi, F. D. Zhang, M. Zhang, and P. D. Ye, "Gas sensing properties of index-guided PCF with air-core," *Optics & Laser Technology*, 2008, 40(1): 167–174.
[32] S. Olyaee and A. Naraghi, "Design and optimization of index-guiding photonic crystal fiber gas sensor," *Photonic Sensors*, 2013, 3(2): 131–136.
[33] S. Olyaee, A. Naraghi, and V. Ahmadi, "High sensitivity evanescent-field gas sensor based on modified photonic crystal fiber for gas condensate and air pollution monitoring," *Optik – International Journal for Light and Electron Optics*, 2014, 125(1): 596–600.
[34] S. Asaduzzaman, K. Ahmed, T. Bhuiyan, and M. F. H. Arif, "Design of simple structure gas sensor Based on hybrid photonic crystal fiber," *Cumhuriyet Science Journal*, 2016, 37(3): 187–196.
[35] X. Yu, Y. Zhang, Y. C. Kwok, and P. Shum, "Highly sensitive photonic crystal fiber based absorption spectroscopy," *Sensors and Actuators: B Chemical*, 2010, 145(1): 110–113.
[36] T. M. Monro, W. Belardi, K. Furusawa, J. C. Baggett, N. G. R. Broderick, and D. J. Richardson, "Sensing with microstructured optical fibres," *Measurement Science and Technology*, 2001, 12(7): 854–858.
[37] M. Morshed, S. Asaduzzaman, and K. Ahmed, "Proposal of simple gas sensor based on micro structure optical fiber," in *IEEE International Conference on Electrical Engineering and Information Communication Technology*, Dhaka, Bangladesh, pp. 1–5, 2015.
[38] J. W. Wang, C. Jiang, W. S. Hu, and M. Y. Gao, "Properties of index-guided PCF with air-core," *Optics & Laser Technology*, 2007, 39(2): 317–321.
[39] N. A. Mortensen, J. R. Folkenberg, M. D. Nielsen, and K. P. Hansen, "Modal cutoff and the V parameter in photonic crystal fibers," *Optics Letters*, 2003, 28(20): 1879.
[40] M. Morshed, M. F. H. Airf, S. Asaduzzaman, and K. Ahmed, "Design and characterization of photonic crystal fiber for sensing applications," *European Journal of Scientific Research*, 2016, 11(12): 228–235.
[41] S. Olyaee and F. Taghipour, "Doped-core octagonal Photonic crystal fiber with ultra-flattened nearly zero dispersion and low confinement loss in a wide wavelength range," *Fiber and Integrated Optics*, 2012, 31(3): 178–185.
[42] S. E. Kim, B. H. Kim, C. G. Lee, S. Lee, K. Oh, and C. S. Kee, "Elliptical defected core photonic crystal fiber with high birefringence and negative flattened dispersion," *Optics Express*, 2012, 20(2): 1385.
[43] P. Ma, N. F. Song, J. Jin, J. M. Song, and X. B. Xu, "Birefringence sensitivity to temperature of polarization maintaining photonic crystal fibers," *Optics & Laser Technology*, 2012, 44(6): 1829–1833.
[44] S. Sen, S. Chowdhury, K. Ahmed, and S. Asaduzzaman, "Design of a porous cored hexagonal photonic crystal fiber based optical sensor with high relative sensitivity for lower operating wavelength," *Photonic Sensors*, 2017, 7(1): 55–65.
[45] S. Asaduzzaman, K. Ahmed, and B. K. Paul, "Slotted-core photonic crystal fiber in gas-sensing application," *SPIE*, 2016, 10025: 100250O1–100250O9.
[46] M. Napierala, T. Nasilowski, E. Beres-Pawlik, F. Berghmans, J. Wojcik, and H. Thienpont, "Extremely large-mode-area photonic crystal fiber with low bending loss," *Optics express*, 2010, 18(15): 15408–15418.
[47] J. Broeng, D. Mogilevstev, S. E. Barkou, and A. Bjarklev, "Photonic crystal fibers: a new class of optical waveguides," *Optical Fiber Technology*, 1999, 5(3): 305–330.
[48] M. N. Petrovich, A. Brakel, F. Poletti, K. Mukasa, E.

Austin, V. Finazzi, *et al.*, "Microstructured fibers for sensing applications," *SPIE*, 2005, 6005: 60050E1–60050E15.

[49] H. H. El, Y. Ouerdane, L. Bigot, G. Bouwmans, B. Capoen, A. Boukenter, *et al.*, "Sol-gel derived ionic copper-doped microstructured optical fiber: a potential selective ultraviolet radiation dosimeter," *Optics Express*, 2012, 20(28): 29751.

[50] H. Ebendorff-Heidepriem, P. Petropoulos, S. Asimakis, V. Finazzi, R. Moore, K. Frampton, *et al.*, "Bismuth glass holey fibers with high nonlinearity," *Optics Express*, 2004, 12(21): 5082.

[51] K. M. Kiang, K. Frampton, T. M. Monro, R. Moore, J. Tucknott, D. W. Hewak, *et al*., "Extruded single-mode non-silica glass holey optical fibers," *Electronics Letters*, 2002, 38(12): 546–547.